

Received: 28 February 2022 / Accepted: 24 April 2022 / Published online: 04 May 2022

*machine tools, robotics, double ball bar,
geometric accuracy, static accuracy*

Johann August MARWITZ^{1*}, Nikolas Alexander THEISSEN²,
Monica Katherine GONZALEZ², Christian FRIEDRICH¹,
Arvid HELLMICH¹, Andreas ARCHENTI²,
Steffen IHLENFELDT^{1,3}

ACCURACY ASSESSMENT OF ARTICULATED INDUSTRIAL ROBOTS USING THE EXTENDED- AND THE LOADED-DOUBLE-BALL-BAR

This research paper outlines the methodology and application of geometric and static accuracy assessment of articulated industrial robots using the Extended Double Ball Bar (EDBB) as well as the Loaded Double Ball Bar (LDBB). In a first experiment, the EDBB is used to assess the geometric accuracy of a Comau NJ-130 robot. Advanced measuring trajectories are investigated that regard poses or axes configurations, which maximize the error influences of individual robot components, and, in this manner, increase the sensitivity for a large number of individual error parameters. The developed error-sensitive trajectories are validated in experimental studies and compared to the circular trajectories according to ISO 203-4. Next, the LDBB is used to assess an ABB IRB6700 manipulator under quasi-static loads of up to 600 Newton using circular testing according to ISO 230-4. The stiffness is identified from the loaded circular trajectories. Then, the stiffness is used to perform a reverse calculation to identify the kinematic errors on the path deviations. The concept is validated in a case study of quasi-static loaded circular testing using the LDBB compared to a Leica AT960 laser tracker (LT).

1. INTRODUCTION

Today, the demand for industrial robots is significant, as shown by their market volume of approximately 13.2 billion USD in 2020, and continuously increasing in the future [1]. Already, industrial robots can realize numerous industrial applications, especially in handling, while providing modern manufacturing environments with the flexibility to adapt to smaller lot sizes at the same time. However, new applications, such as machining, as well as a wider usage of offline programming require a higher positioning accuracy of industrial robots [2]. The improvement of positioning and path positioning accuracy [3], as a measure for the distance between the commanded and the attained position of a manipulator, is subject to

¹ Fraunhofer Institute for Machine Tools and Forming Technology, Dresden, Germany

² KTH Royal Institute of Technology, Stockholm, Sweden

³ Institute of Mechatronic Engineering, Chair of Machine Tools Development and Adaptive Controls, TU Dresden, Germany

* E-mail: johann.marwitz@iwu.fraunhofer.de

<https://doi.org/10.36897/jme/149413>

the study of manipulator calibration [4], whereby an essential step of manipulator calibration is the accuracy assessment by measurements. In this context, measurement is the multi-level process of experimentally obtaining end-effector poses (defined as combined position and orientation [3]) that can be used to identify and implement model parameters for the optimised operation of the industrial manipulator. The most important aspects of the measurement procedure are the ability to measure unconstrained arbitrary trajectories as well as the measurement instrument itself. Hereby, the error sources of the pose deviation can be classified into geometric or kinematic errors, elasto-static errors, and thermal errors.

First, geometric or kinematic calibration focuses on the deviation of the pose of the end-effector as a consequence of the imperfect geometries of the components, the assembly, or the configurations regarding the Denavit Hartenberg (DH) parameters without further consideration of solid mechanics in terms of forces and torques, or thermodynamics in terms of heat affecting the mechanical structure [5]. In general, depending on the specific scenario of machine evaluation, such as machine comparison, quality acceptance assessment, or machine diagnostics, different efforts and financial costs are acceptable [6]. For this reason, many measurement instruments and approaches focusing on kinematic calibration with different accuracies and cost have been studied since the beginning of geometric error evaluation.

The benchmark measurement instrument for kinematic manipulator calibration are laser trackers, also called tracking laser interferometers. These were invented in the 1980s and are now commercially and widely available [7]. They are widely accepted, as they are accurate, i.e., the uncertainty associated with the measurement is often less than 1/10 of the manipulator's repeatability. They are versatile, i.e., they offer to perform simple static point measurements to continuous pose measurement at commonly 1000 Hz. Finally, laser trackers are user-friendly, i.e., the latest version can be easily transported and setup. Nevertheless, their high cost with a price of approximately 130 000 € and the lack to perform calibration on the site of the customer have inspired research for complementary measurement instruments.

Alternative measuring systems are based on specific reference artefacts, such as ball plates, precision spheres, or cross grids, that are evaluated by linear gauges, touch probes, or grid encoders [6]. However, these methods are limited to single poses or axes, require significant installation efforts, and are expensive when regarding the precision reference artefacts. Contact based measurement instruments that do not significantly constrain the trajectory are for example the CompuGauge by Dynalog [8] or the LaserTracer MT by Etalon [9]. Measurement instruments that constrain the trajectory but are non-contact based are interferometers [10], and, finally, measurement instruments that do not constrain the trajectory and are non-contact based can be found in photogrammetry systems [11] or LaserTracers. Then other measurement instruments, such as the conventional Double Ball Bar (DBB), can be used for contact-based measurement of constrained trajectories [12]. However, due to the limited measuring range of commonly ± 1.5 mm [13], the trajectory is limited to a circle or a sphere.

The DBB concept has also been developed in notable works such as the Laser Ball Bar (LBB) by Ziegert and Mize [14] to measure positioning accuracy through the application of trilateration or as well as the the High Precision Telescopic Instrument (HPTI) by Brosted et al. [15].

The Extended Double Ball Bar (EDBB) is, as the DBB, a length measuring system that measures the distance between two balls, whereby one ball is fixed to the base by a magnetic 3-point-fixture and the other ball is moved by the robot. As no ideal machine exists, the difference between the nominal and the actual ball distance contains the motion error of the robot in 6 degrees of freedom (DOF), which is projected to a one-dimensional subspace by the length measurement. The EDBB can be considered as a conventional DBB regarding the measurement concept, the measurement instrument price in the range of 5 000 to 10 000 €, and the ease of use. However, since its measuring range is up to 220 mm, it does not constrain the trajectory significantly. To achieve a wide range with high accuracy, the EDBB consists of a linear measuring system with incremental encoder and contactless optical sensor that is mounted on a linear miniature guide within an invar steel and carbon housing, Fig. 1. Based on a scale of 20 μm , by 50 times interpolation and 4 times evaluation a resolution of 0.1 μm and accuracy of 1 μm is realised [6].

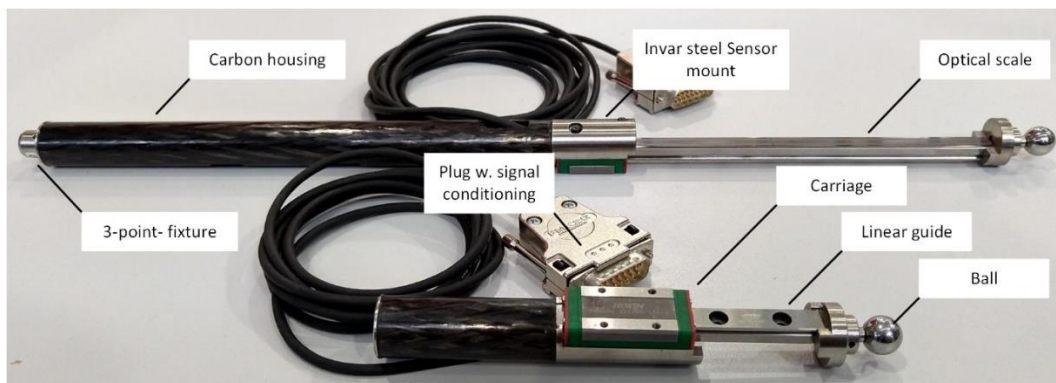


Fig. 1. Extended Double Ball Bars with different measuring range, developed at the TU Dresden [6, 16, 17]

Next, the measurement of elasto-static errors, as pose deviations due to the compliance of the robot and its components, shall be discussed. In order to evaluate the compliance of the robot and its components, the deviation of the end-effector pose must be measured in load situations. One main approach is to apply a known mass to the robot and compare deviation measurements without and with mass to eliminate geometric error components. By temperature sensing and repeated DBB measurements with fixed measuring periods for each load situation, also thermal effects can be eliminated [18]. Another approach is to apply the force by the measuring system itself, as realised here and described below. A summary of further instruments and approaches is given in the work of Garnier et al. [19].

The Loaded Double Ball Bar (LDBB) is a tool for quasi-static loaded circular testing of machine tools and industrial manipulators based on a one dimensional deflection measurement introduced by [20]. The LDBB has a pneumatic actuator inbuilt to regulate the magnitude of force applied, Fig. 2. When pressurized air is injected into the instrument's cylinder, a mechanical force is generated, which causes the deflection of the mechanical structure [21]. Static load and distance between the tool and table ball are measured at the same time by a pressure sensor and a single linear variable differential transformer, respectively [22].

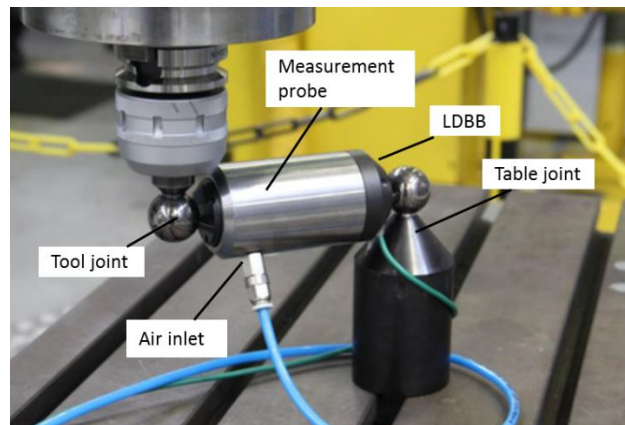


Fig. 2. Loaded Double Ball Bar for loaded circular testing, developed at KTH Stockholm [21, 23]

This research work identifies limitations and disadvantages of measurement instruments for industrial manipulator calibration, and it supports developments towards new measurement instruments to overcome. In that the manuscript highlights the potential of contact based unconstrained measurement for the identification of kinematic and compliance errors. However, there is still no such device. This article scrutinises the measurement instruments for the contact based unconstrained measurement for the assessment of kinematic errors (EDBB), and the contact based constrained measurement for the assessment of compliance errors (LDBB), to propose a measurement instrument for the identification of kinematic and compliance errors. The EDBB and LDBB are the subject of this investigation, as both measurement instruments are similar to the DBB, i.e., the measurement procedures are fast, simple, and robust. This accretion is based on the assumption that there are more industrial practitioners with proficiency in ball bar testing, rather than optical or laser-based measurement procedures.

This contribution is structured in the following way: First, the methodology is presented for a measurement with the EDBB and the LDBB (Section 2). For the EDBB with its complex measuring path this includes the implementation of the kinematic model, a sensitivity analysis, and the path generation. As the LDBB moves along a circular path due to its limited range, path preparation is much simpler in this case. Next, the experimental setup is presented for both, the EDBB and the LDBB, with different robots (Section 3) and, finally, the measuring results are evaluated (Section 4).

2. METHODOLOGY

2.1. GEOMETRIC ERROR EVALUATION WITH THE EDBB

Geometric errors on serial manipulators can be caused by assembly and manufacturing tolerances, as well as by axis zero position errors due to incorrect mastering. In order to make the various error influences on the deflection of the manipulator's end-effector visible, a kinematic model of the manipulator and the measurement setup is used for a sensitivity analysis. This is latter on referred to the kinematic measurement model.

On this basis, a trajectory can be generated. By filtering a global set of poses with respect to error sensitivity, collision freedom, working space limits of the EDBB and constraints caused by the wiring harness, the optimal poses as well as the necessary number of poses are determined. These are then rearranged to generate the shortest possible trajectory in terms of travel time. First, the measurement model for the sensitivity analysis is described, followed by the trajectory generation.

2.1.1. KINEMATIC MEASUREMENT MODEL

For the sensitivity analysis, an equation is required that describes the length of the EDBB as a function of the joint angles \mathbf{q} and the geometric parameters \mathbf{p} of all elements in the structural loop. This equation results from the concatenation of parameter-dependent homogeneous transformation matrices, Fig.:

1. the forward transformation from the base frame $\{b\}$ to the flange frame $\{fl\}$ ${}^b\mathbf{T}_{fl}(\mathbf{q}, \mathbf{p}_{DH})$ as a function of 6 joint angles \mathbf{q} and 24 standard DH-parameters \mathbf{p}_{DH} [24],
2. the transformation ${}^{fl}\mathbf{T}_{map}(x, y, z)$ from the flange frame $\{fl\}$ to the measurement application point $\{map\}$, respectively, as a function of displacement (3 parameters),
3. and the transformation ${}^{fix}\mathbf{T}_b(x, y, z)$ from the EDBB fixture frame $\{fix\}$ to the base frame $\{b\}$ of the manipulator, as a function of the displacement (3 parameters).

These three matrices can be used to express the distance between the $\{map\}$ - and the $\{fix\}$ -frame, which is measured by the EDBB.

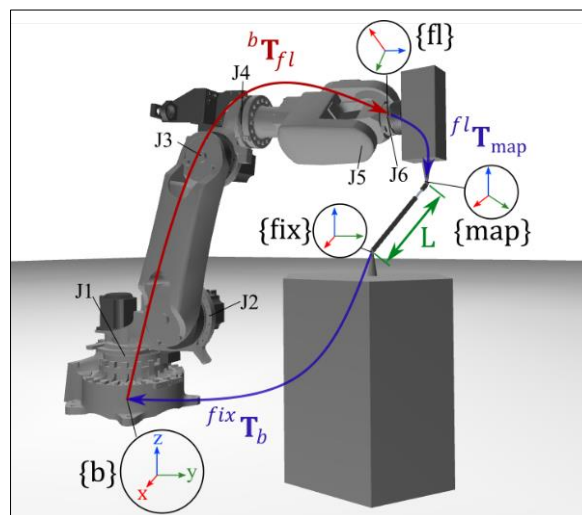


Fig. 3. Transformations of the kinematic measurement model

The nonlinear multidimensional target function of the measured variable depending on 30 geometric model parameters and six joint angles results as follows:

$${}^{fix}\mathbf{T}_{map}(\mathbf{q}, \mathbf{p}) = \begin{bmatrix} {}^{fix}\mathbf{R}_{map} & {}^{fix}\mathbf{t}_{map} \\ \mathbf{0} & 1 \end{bmatrix} = {}^{fix}\mathbf{T}_b \ {}^b\mathbf{T}_{fl} \ {}^{fl}\mathbf{T}_{map}. \quad (1)$$

$$L = f(\mathbf{q}, \mathbf{p}) = \|{}^{fix}\mathbf{t}_{map}\|_2 \quad (2)$$

To quantify the sensitivity of the model parameters \mathbf{p} on the measurement result for a given set of joint angles \mathbf{q}_0 , the objective function can be linearized around the assumed model parameters \mathbf{p}_0 by neglecting higher order error terms:

$$\tilde{L} = f(\mathbf{q}_0, \mathbf{p}_0) + \frac{\partial f(\mathbf{q}_0, \mathbf{p})}{\partial p_1} \Delta p_1 + \dots + \frac{\partial f(\mathbf{q}_0, \mathbf{p})}{\partial p_n} \Delta p_n. \quad (3)$$

The influence of the geometric perturbations on the measurement result can thus be described as follows:

$$\Delta m = \tilde{L} - f(\mathbf{q}_0, \mathbf{p}_0) = \nabla f(\mathbf{q}_0, \mathbf{p}) \Delta \mathbf{p} = \mathbf{j} \Delta \mathbf{p}, \quad (4)$$

where Δm denotes the error between measured and computed EDBB length, $\Delta \mathbf{p}$ is a column vector describing the perturbations of the parameters of the kinematic measurement model $\Delta \mathbf{p} = [\delta\theta_1 \ \dots \ \delta\alpha_6]$, and \mathbf{j} is a row vector describing the amplification of the perturbations. The relationship could be derived either analytically or numerically by using approaches such as finite difference and algorithmic differentiation [17].

Information from different measurements in different joint angle sets $\mathbf{q}_0 \dots \mathbf{q}_n$ is collected and combined by stacking n equations into a matrix form:

$$\Delta \mathbf{m} = \mathbf{J} \Delta \mathbf{p}, \quad (5)$$

where the matrix $\mathbf{J} \in \mathbb{R}^{n \times m}$ names identification Jacobian in literature [23].

2.1.2. PARAMETER ANALYSIS

Table 1 shows the nominal DH parameters of the Comau NJ-130 manipulator used for the sensitivity analysis. The values θ_i are to be interpreted as joint angle offsets, whereas the joint angles are represented by the vector \mathbf{q} . The scaling of the input vectors \mathbf{q} and \mathbf{p} was neglected, since radian and meter are comparable for this current robot size and geometrical modelling [25, 26]. The Comau NJ-130 manipulator used for the evaluation belongs to this category.

Table 1. Nominal DH-parameters according to [24] of the Comau NJ-130 manipulator

i	α_{i0} [rad]	a_{i0} [m]	d_{i0} [m]	θ_{i0} [rad]
1	$-\pi/2$	0.4	0.55	0
2	$-\pi/2$	0.86	0	$-\pi/2$
3	$-\pi/2$	-0.21	0	π
4	$-\pi/2$	0	0.76158	π
5	0	0	0	0
6	0	0	0.21	$-\pi/2$

Before using the identification Jacobian for sensitivity analysis, all linearly dependent parameters and all parameters whose change has none or only little influence on the measurement result must be set to a fixed value. For this objective, the QR decomposition or the singular value decomposition (SVD) of the identification Jacobian can be used [26]. By using SVD for the specific model, eight redundant or negligible parameters were identified. Eqn. (6) shows the full model parameter vector before eliminating the dependencies.

$$\mathbf{p} = [x_{\text{fix}}, y_{\text{fix}}, z_{\text{fix}}, \alpha_1, \dots, \alpha_6, a_1, \dots, a_6, d_1, \dots, d_6, \theta_1, \dots, \theta_6, x_{\text{map}}, y_{\text{map}}, z_{\text{map}}], \quad (6)$$

The following parameters have been set to fixed values:

1. The three translational parameters to describe the MAP ($x_{\text{map}}, y_{\text{map}}, z_{\text{map}}$), which are linearly dependent to the DH parameters of the last link (α_6, a_6, d_6).
2. The three translational parameters to describe the fixture ($x_{\text{fix}}, y_{\text{fix}}, z_{\text{fix}}$), which are not part of the manipulator.
3. The DH-parameters d_2 and d_3 are linearly dependent because the joint 2 and 3 are arranged in parallel (Fig. 3).
4. The joint angle offset Θ_6 , as only position information regarding the MAP is recorded by means of the EDBB. These can be described in only three parameters, in this case α_6, a_6 and d_6 .

The target function Eq. (2) is thus reduced from 30 to 22 geometric model parameters.

In order to evaluate the quality of pose sets with respect to the amplification of geometric errors, a criterion is required. In the field of robot calibration, the observability index is used for this purpose. It characterizes the sensitivity of constraint equations to variation in the kinematic parameters [27]. The identification Jacobian, Eq. (5), is a function of the measurement configuration for a particular set of poses, hence optimization of its observability index $O(\mathbf{J})$ results in higher sensitivity with respect to kinematic perturbations $\Delta\mathbf{p}$ in the observation $\Delta\mathbf{m}$ [27].

There are different approaches to determine the observability index, Table 2, which describe different quality criteria. Basically, two criteria are to be fulfilled [17]:

1. The kinematic perturbations $\Delta\mathbf{p}$ should be amplified as strong as possible on the observer $\Delta\mathbf{m}$ to suppress non-kinematic effects.
2. The kinematic perturbations $\Delta\mathbf{p}$ should be amplified equally in all dimensions on the observer $\Delta\mathbf{m}$ for the effects to be represented identically in the measurement.

Table 2. Observability indices, $\mu_1 \dots \mu_r$ are the singular values of the identification Jacobian \mathbf{J} , which represent the semiaxes of a hyper ellipsoid [25, 26]

Index	Expression	Name	Description
O_1	$\frac{\sqrt[r]{\mu_1 \dots \mu_r}}{\sqrt{P}} \rightarrow \max$	The Product of Singular Values	Represents the volume of a hyper ellipsoid P is the number of poses.
O_2	$\frac{\mu_1}{\mu_r} \rightarrow \min$	The Condition Number	Measures the eccentricity of the hyper ellipsoid.
O_3	$\mu_r \rightarrow \max$	The Minimum Singular Value	Measures the size of the minimum axis of the hyper ellipsoid.
O_4	$\frac{\mu_r^2}{\mu_1} \rightarrow \max$	The Noise Amplification Index	Measures both the eccentricity of the ellipse through O_2 as well as the size of the ellipse through O_4 .

Ruiqing et. all have shown in [17] that the use of the condition number of the identification Jacobian as observability index best satisfies the two criteria. Therefore, O_2 (Table 2) is applied for the sensitivity analysis in the trajectory generation.

2.1.3. PATH GENERATION

For the automatic generation of optimal measurement trajectories, several steps are necessary which will be explained in the following. Initially, some configurations must be prepared. First, the kinematic model of individual manipulators needs to be defined, which includes the nominal DH parameters (according to Table 1), as well as the MAP (displacement between fixture and flange). This is necessary for the sake of the sensitivity analysis and the pose generation by means of forward transformation from the joint angles (minimal coordinates). Next, the measurement space for the trajectory must be determined, by specifying the position of the stationary fixture, the EDBB length and the EDBB measurement range. This results in a workspace in the shape of a spherical shell which is arranged relative to the manipulator. Optimally, the joint angle space should be constrained to the measurement space to reduce the computation time during pose generation. Since the joint angles represent the minimal coordinates, which means they are independent of each other and not redundant, uniformly distributed configurations are generated within the joint space and transferred into the task space by forward transformation. The distribution step size must be defined as a compromise between computation time and resolution of the discretization.

This initially large set of equidistant axis angle configurations is transformed to the task space and then filtered for all poses outside the measurement space, poses that cause a collision between manipulator, tool, cables, environment or EDBB placement. Figure 4a shows approximately 3400 valid poses in the EDBB measurement space. The number of poses is based on a heuristic approach which trades time and quality based on the acceptable computational cost in the sensitivity analysis.

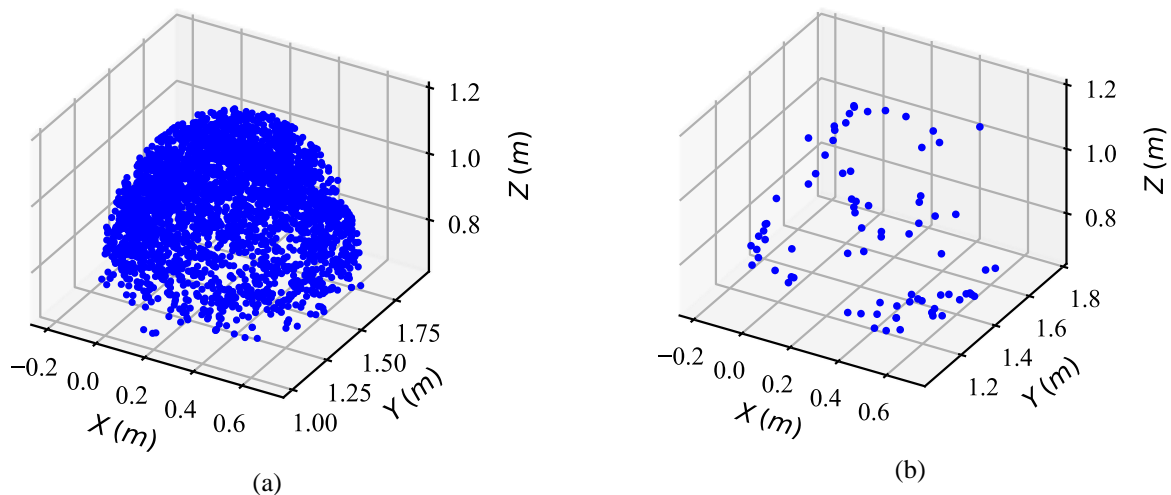


Fig. 4. Initial pose set – (a), final pose set – (b)

To analyse the sensitivity of a set of poses, the identification Jacobian, cf. Eq. (5), is calculated numerically. The central difference quotient with a step size of $1/3$ of the computer accuracy is used ($h = 1/3 \varepsilon$). If n is the number of poses and m the number of observed error effects, the identification Jacobian has the dimension $\mathbf{J} \in \mathbb{R}^{n \times m}$. Iteratively, poses are sorted out which lead a worse observability index (O_2 : condition number) and thus to a poor sensitivity with respect to the kinematic perturbations. This is repeated until the number of poses is reduced to the number of parameters ($n = m$). Figura 5 shows the progression of the condition of \mathbf{J} over a portion of the number of poses. For the individual test carrier Comau NJ-130, it can be seen that an optimum number of poses is reached at approx. 35. For the trajectory generation, however, it has proven to be useful to use a large number of poses to reduce the collisions caused by joint interpolation (Fig. 4b).

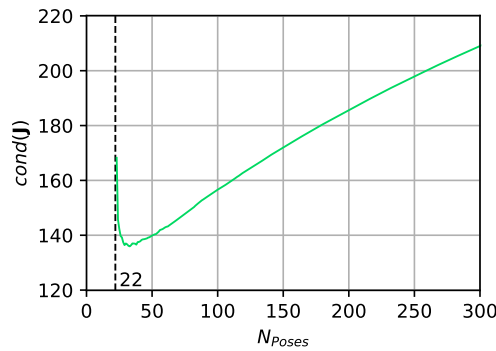


Fig. 5. Condition of orthogonalized Jacobi matrix optimized with iterative algorithm

Finally, for the generation of the measurement trajectory, the determined sensitive set of poses should be rearranged with respect to the travel time. As described in [17], this optimization task can be described as a traveling salesman problem (TSP). For this purpose, a cost matrix must be created that quantifies the effort required to move between the individual poses of the complete set. Different from [15] where the length of a path between two cartesian positions is applied, the movement time of the slowest axis in a joint movement estimated by means of the following time optimal criterion is used:

$$c_{ij}(\mathbf{qi}, \mathbf{qj}) = \max_{n=1, \dots, 6} \frac{|q_n^i - q_n^j|}{\omega_n}, n \in \mathbb{N}. \quad (7)$$

The vector \mathbf{qi} represents start joint positions, the vector \mathbf{qj} represents of end joint positions and the vector $\boldsymbol{\omega}$ represents of maximal joint speeds. This work used the established concord TSP [28] solver, which is considered to be particularly fast. By rearranging the poses using TSP, the estimated time could be reduced from about 240 s to about 22 s (cf. Fig. 6).

After the optimal sequence of poses has been found, a joint interpolation between the axis configurations is performed. A new analysis is carried out to determine whether the interpolation would cause workspace violations, collisions, or damage to the wiring. To eliminate these problems, new support poses are automatically inserted into the trajectory. Finally, the generated measurement trajectory is slightly blended in task space by 10 mm in order to achieve a faster measurement movement, a more consistent speed and to avoid jerk. To provide the trajectory to the robot controller, G-code is generated. Figure 7 shows the specific error-sensitive measurement path on the Comau NJ-130 test carrier.

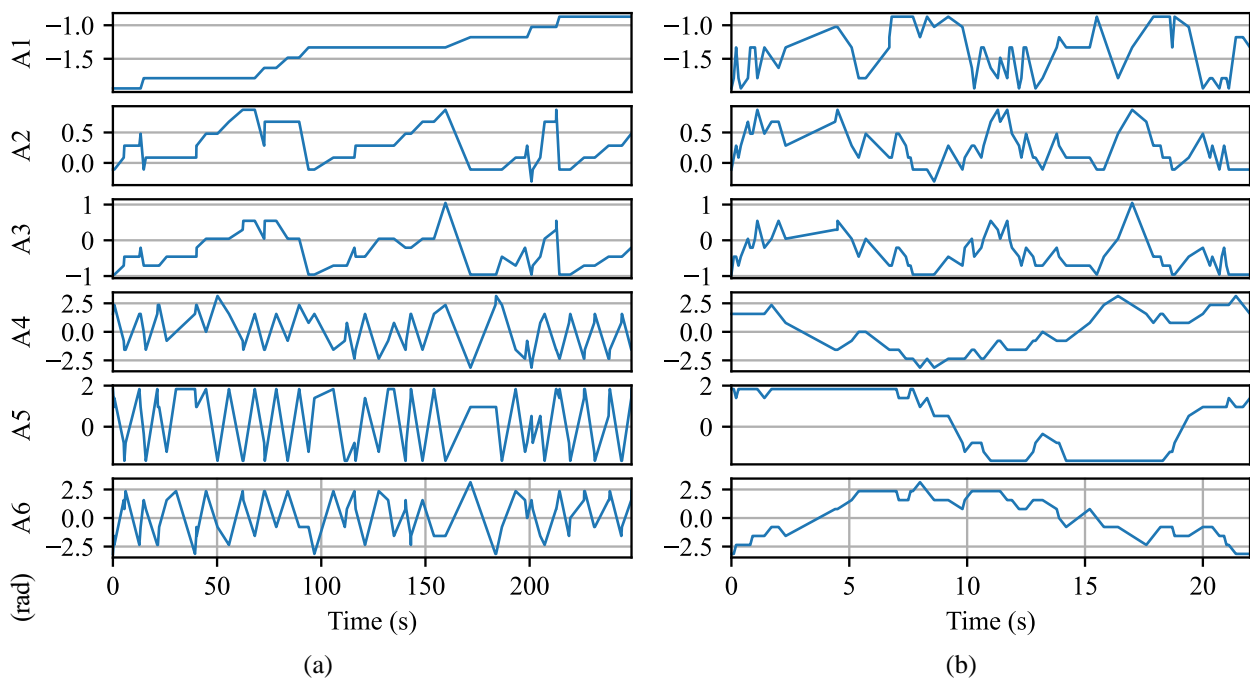


Fig. 6. Joint position trajectories over estimated time: (a) for unsorted poses, (b) for sorted poses

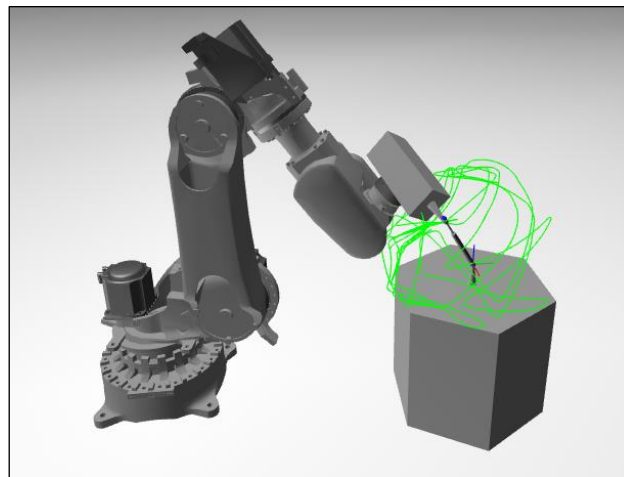


Fig. 7. Visualisation of an error-sensitive trajectory on the Comau NJ-130

2.2. COMPLIANCE ERROR EVALUATION WITH THE LDBB

The procedure measures quasi-static deflections, i.e., deflections of the manipulator’s end-effector under movement along a circular trajectory [29]. The conceptual measurement setup is delineated in Fig. 8. The robot is programmed to move along a single circular trajectory.

The first metrology loop uses a linear variable differential transformer (LVDT) inside the LDBB for the deflection measurement [30]. The second metrology loop uses the LT. The LT measurement data serve as a reference standard for the validation of the LVDT data.

The transformation of the LT data into the robot base coordinate system (RBCS) is based on the circle point method [4]. The transformation of the LDBB data into the RBCS is based on the procedure described in [31]. For both, the static and the quasi-static measurement, multiple force components were exerted simultaneously. This approach differs from the description of circular testing according to ISO 230-4. Thus, the Z-axis component's magnitude was chosen to be approx. 1/3 of the total load, while the remaining 2/3 were split between the X- and Y-axis components (Fig. 8). The contribution of the X- and Y-axis components depended on the position of the LDBB along the circular trajectory.

All measurements with the LDBB feature a mechanical base load reference (MBLR), i.e., the compliance based deflections are not derived as the difference between an unloaded and a loaded configuration but as the difference of a loaded configuration with respect to another loaded configuration. This approach can also be considered as a pre-loading of the components in the force loop. This action is meant to reduce errors in the measurement resulting from play or backlash and minimise the instrument uncertainty.

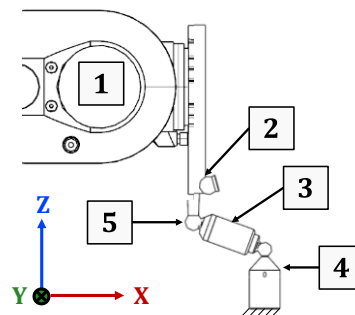


Fig. 8. Conceptual scheme for the quasi-static loaded circular testing measurement setup: 1) large-sized articulated industrial robot, 2) a Leica AT901-LR LT (represented through the 0.5 in spherical retroreflector), 3) the measurement instrument LDBB, 4) rigid table link, and 5) an end-effector with the tool centre point

3. EXPERIMENTS

3.1. GEOMETRIC ERROR EVALUATION

The experimental measurement setup is delineated in Fig. 9 and consists of the following components:

1. Serial articulated industrial robot Comau NJ-130, payload 130 kg and reach 2.05 m, with a B&R controller and integrated CNC core (not included in the picture),
2. Measurement instrument Extended Double Ball Bar (EDBB) [6] with a measuring range of 220 mm and an accuracy of 1 μm ,
3. Fixture with adjustable zero point from Renishaw.

End-effector with measurement application point. The fixture is approx. at a position $P = [258 \ 1468 \ 708]^T$ mm within the RBCS. Initially, the robot is moved to this position with its MAP and the zero point is adjusted with the help of a calibration ball on the fixture.

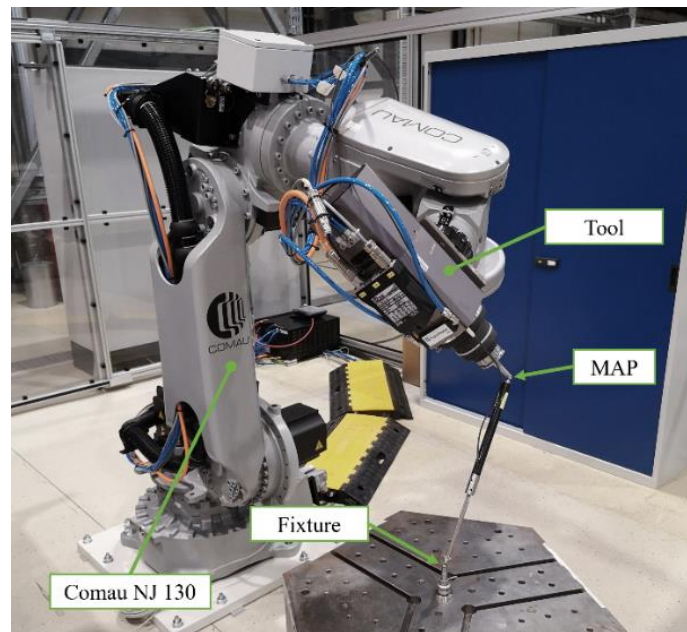


Fig. 9. Measurement setup for the geometric error evaluation

Firstly, the robot is programmed to move along a bidirectional circular trajectory in the XY-plane and bidirectional half circular trajectory in the XZ- and YZ-plane. The diameter of the circle is approximately 700 mm. The trajectory can be seen as an extended circular test according to DIN ISO 230-4. Secondly, the robot is programmed to move along the automatically generated error-sensitive trajectory.

The task space velocity is set to 1000 mm/min for both the circular trajectory and the error-sensitive trajectory to suppress non-geometric error influences as far as possible. All joint angles are recorded synchronously with the deflection of the EDBB. The sampling time corresponds to 2 ms, whereby all values are provided with a time stamp accurate to 50 μ s. The joint angles are linearly interpolated to the time stamp of the EDBB.

3.2. COMPLIANCE ERROR EVALUATION

The experimental measurement setup is delineated in Fig. 10. The robot is programmed to move along a single circular trajectory with a diameter of approximately 250 mm, which is centred at a position $P = [1350 \quad -125 \quad 1250]^T$ within the RBCS. The setup is depicted in Fig. 10 and it comprises the following equipment:

1. Serial articulated industrial robot, payload 300 kg and reach 2.7 m, with its corresponding controller (not included in the picture),
2. Leica AT901-LR Laser Tracker (LT) (not included in the picture) with a 0.5 in Spherically Mounted Retroreflector (SMR),
3. Measurement instrument Loaded Double Ball Bar (LDBB) [32] with a co-axially installed DTA-3G8-3-CA LVDT
4. Rigid table link,
5. End-effector with tool centre point.

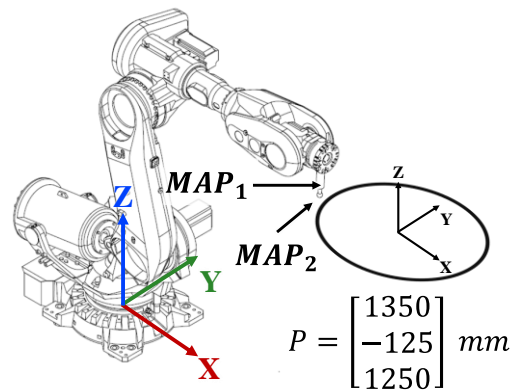


Fig. 10. Measurement setup for the compliance error evaluation. The figure does not correctly depict the position of the circle

The deflection measurements are performed with two different metrology loops [33]. The first metrology loop uses an LVDT for the deflection measurement. The second metrology loop uses the LT. The LT measurement data serve as a reference standard for the validation of the LVDT data. The distance between the MAPs, also called points of interest, of the LVDT and the LT equals approximately 6 mm. Figure 10 shows the MAPs of the LT as MAP_1 and the of the LVDT as MAP_2 .

The quasi-static loaded circular measurement procedure induces loads of 125 N, 250 N, 375 N, 500 N, and 625 N along a single circular trajectory. Then, the manipulator moves two times clockwise about the same circular trajectory, see Fig. 10. The circles were measured with an angular overshoot of 180° to exclude transient effects from the measurement data. The manipulator followed the trajectory with a Cartesian velocity of 50 mms^{-1} . The LT and the LVDT are set to continuous data recording at 1,000 Hz, which dissected the circle into 15,899 measurement points. The points are spaced at a distance of approximately $50 \mu\text{m}$ along the circumference of the circle. This minimises errors in the data analysis. This will be further discussed in the results section.

4. RESULTS

4.1. GEOMETRIC ERROR EVALUATION

Figure 11 shows the EDBB distance for the extended circular test (a) and for the error-sensitive trajectory (b) in red. The extended circle test uses 2.45 mm of the measuring range of the EDBB, which nearly exceeds the measuring range of a conventional DBB of approx. $\pm 1.5 \text{ mm}$ [13]. The error-sensitive trajectory uses 156.32 mm of the measuring range. The measurement time for the error-sensitive trajectory is approximately twice that of the extended circular test. Overall, the traversing speed could be increased significantly and thus the measurement duration shortened considerably. In order to suppress non-geometric error influences as far as possible, a relatively slow speed was deliberately chosen here (cf. Section 3.1).

In addition to the measured distance (red), the calculated deflection based on the joint angle setpoints is shown in green and the calculated deflection based on the actual joint angle values is shown in blue. It can be noticed that a deviation of up to 0.5 mm in the EDBB deflection occurs due to the contouring error.

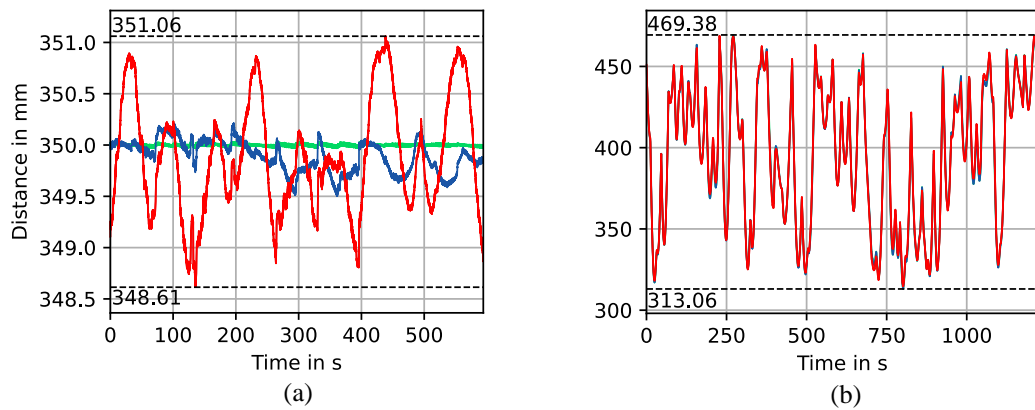


Fig. 11. Calculated and measured distance of the MAP to the stationary EDBB fixture: (a) extended circular test according to DIN ISO 230-4, (b) error sensitive generated trajectory

In order to make the two trajectories comparable and to suppress the deviation of the deflection due to the contouring error, the deviation between the calculated (based on the actual axis values, blue) and measured distance is shown in Fig. 12. It is visible that the extended circularity test leads to a deviation in the range of 2.36 mm. In comparison, with the error-sensitive trajectory, a deviation of approx. 3.5 times is observed, in a range of 8.28 mm.

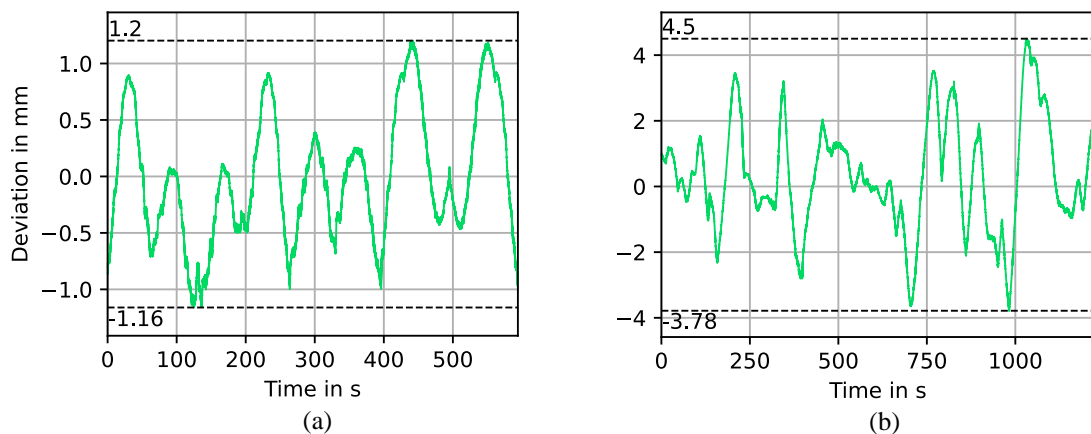


Fig. 12. Deviation between calculated and measured EDBB distance: (a) extended circular test according to DIN ISO 230-4, (b) error sensitive generated trajectory

This shows that a trajectory sensitive to geometric error influences which uses a large measuring range of the EDBB reflects the kinematic perturbations much better. With regard to the method presented in Section 2.1 for the automatic generation of trajectories, it is therefore possible to represent the path accuracy of industrial robots more correctly. This

creates the possibility for a quick, cost-efficient and simple evaluation of accuracy on the ready to run industrial robot with the help of the EDBB. In future work, kinematic calibration of industrial robots can be investigated on this basis.

4.2. COMPLIANCE ERROR EVALUATION

The evaluation of the compliance error is based on the relative difference between the loaded trajectories. First, one identifies the compliance induced deflections from the raw data according to:

$$\Delta x_{i,k} = \Delta x_{i,j=[250N:125N:625N]} - \Delta x_{i,j=125N} \quad (8)$$

Here $i \in \mathbb{N}^{1 \times 15899}$ denotes the index of the points along the trajectory and $j \in \mathbb{N}^{1 \times 5}$ denotes the magnitudes of the applied mechanical loads. The raw data can be seen in Fig. 13 (a) and represents the average of five repeated measurements. The resulting differences $\Delta x_{i,k}$ are defined as the deflections at the k apparent load (AL) of 125 N, 250 N, 375 N, and 500 N. In that context an AL of 125 N indicates that considered difference is calculated as the difference of two circular trajectories that have a nominal load difference of 125 N, e.g., the circular trajectory at 250 N with respect to the one at 125 N. The force induced deflections at the different ALs can be seen in Fig. 13 (b).

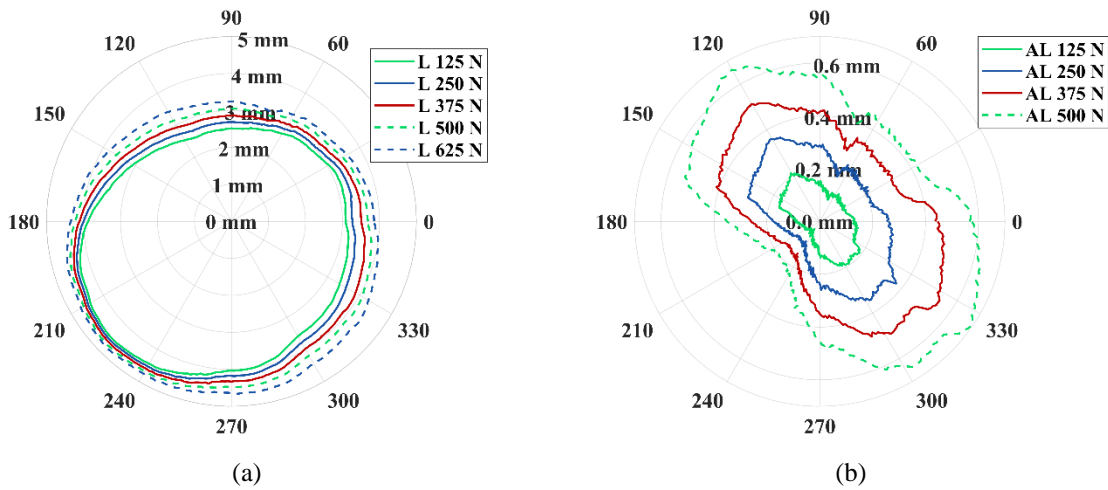


Fig. 13. Measurement data from the LDBB: (a) measurement raw data, (b) compliance induced deflections along the circular trajectory

Then the force induced deflections are subtracted from the trajectories to obtain the compliance compensated trajectories, which can be seen in Fig. 14 (a). Dependent on the linearity of the compliance one would expect all measurement data to ideally coincide on the same line. However, this is not exactly true for this case study, see Fig. 14 (a). The maximum difference between all trajectories equals approx. 180 μm . Then, the average compliance compensated trajectory can be calculated from the individual trajectories, see Fig. 14 (b).

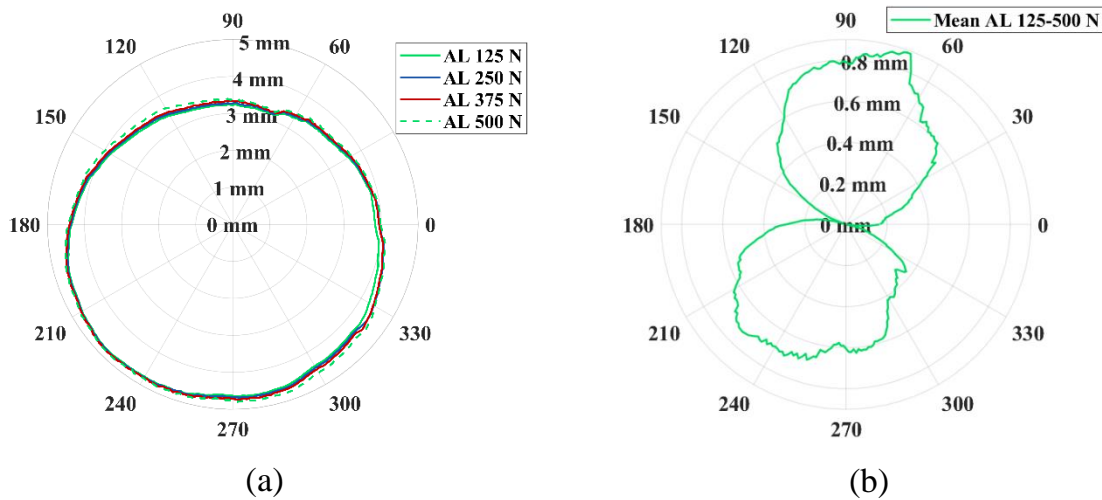


Fig. 14. Compliance compensated trajectories at the AIs – (a), the averaged compliance compensated trajectory – (b)

Finally, it is noticeable that the average compliance compensated trajectory is dominated by an error that takes the shape of a trigonometric function. The majority of this error depends on the offset between the circle centre and the table link, i.e., the centring procedure, and there are minor error components resulting from the eccentricity of the spheres themselves. The offset of the circle can be corrected for using a non-linear least-square approximation of a sinusoidal function, here denoted as $\sin(a, b, \varphi)$, according to:

$$\|a * \sin(b\theta - \varphi) - \bar{y}(\theta)_{meas}\|^2. \tag{9}$$

The identification uses an initial guess of $a = 0.8$ mm for the amplitude, $b = 1$ for the frequency, and $\varphi = 22.5$ deg for the phase shift. The non-linear least squares fitting identifies the following parameters for the case study: of $a = 0.764$ mm for the amplitude, $b = 0.933$ for the frequency, and $\varphi = 14.08$ deg.

Then, the backward calculated kinematic error can be computed as the difference between the averaged compliance compensated trajectory and the function $\sin(a, b, \varphi)$. The result of this calculation can be seen in Fig. 15.

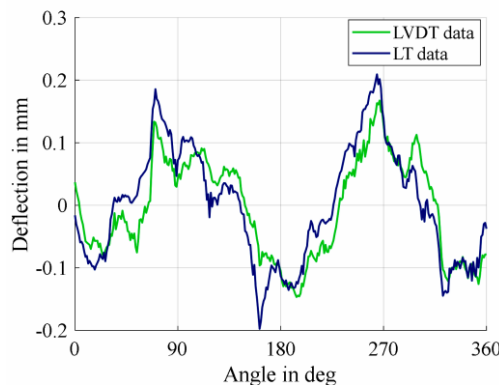


Fig. 15. Compliance and offset compensated average trajectory of the LVDT data compared to an unloaded trajectory measured with a laser tracker, i.e., the kinematic reference error

The average difference between the calculated data from the LDBB and the pure kinematic error measurement from the laser tracker equals approximately 40 μm . As can be seen from the average difference as well as the trend in Fig. 15, after compensating the measured deflections for the compliance as well as the offset of the circle centre, the resulting data yields indicative information about the kinematics of the industrial manipulator. The remaining 40 μm difference is small under the consideration that the error has not been measured at the same MAP. Furthermore, it needs to be highlighted that to obtain the kinematic data no additional information is required, as the data have been backwards calculated from the compliance trajectories. Nevertheless, it is not certain that this will always be the case, as a majority of the error depends on the centring of the circle and there can be scenarios in which the non-linear least-squares fit may result in an erroneous identification, for example if the initial guess is misleading.

5. CONCLUSION

The improvement of the accuracy of industrial robots is one of the main challenges limiting the widespread application of offline programming. This article presented the methodology and application of geometric and static accuracy assessment of serial articulated industrial robots using the Extended Double Ball Bar (EDBB) as well as the Loaded Double Ball Bar (LDBB). Two case studies assessed the geometric accuracy of a Comau NJ-130 robot and the elasto-geometric accuracy of an ABB IRB6700 manipulator using the EDBB and the LDBB.

The experimental results highlighted that both, the geometric and the compliance, errors can be decisive for the successful implementation of industrial robots. The results indicated that a measurement instrument, which can simultaneously measure arbitrary trajectories for geometric and compliance errors, may provide industrial practitioners with added value to their industrial manipulators. Industrial practitioners can assess their manipulators performance in a fast and robust manner, while the data might be used to perform elasto-geometric calibration of the manipulators model parameters. Thus, for the investigated case studies, by identifying the kinematic and quasi-static error it is plausible to achieve a significant and reliable compensation that is more suitable for industrial implementation and potential inclusion by manufacturers of manipulators.

Further research will explore the applicability of such a measurement instrument which may have a considerable impact on positioning accuracy. This in turn can lead to added value through off-line and on-line compensation.

ACKNOWLEDGEMENTS

The authors are grateful to the KTH Royal Institute of Technology and the Fraunhofer Institute for Machine Tools and Forming Technology to allow for this constructive cooperation. Further, the authors want to thank the Institute of Mechatronic Engineering, TU Dresden, for the rental of the EDBB, and, finally, the authors want to thank the editors and reviewers for their helpful comments and constructive suggestions with regard to the revision of this paper.

REFERENCES

- [1] IFR, 2021, *IFR presents World Robotics 2021 reports*, <https://ifr.org/ifr-press-releases/news/robot-sales-rise-again> (accessed: Nov. 9, 2021).
- [2] IBARAKI S., THEISSEN N.A., ARCHENTI A., ALAM M.M., 2021, *Evaluation of Kinematic and Compliance Calibration of Serial Articulated Industrial Manipulators*, *Int. J. Automation Technol.*, 15/5, 567–580, DOI: 10.20965/ijat.2021.p0567.
- [3] ISO-9283, 1998, *Manipulating industrial robots – Performance criteria and related test methods*, Genf: International Organisation for Standardisation.
- [4] MOORING B., ROTH Z.S., DRIELS M.R., 1991, *Fundamentals of Manipulator Calibration*, New York, Wiley.
- [5] VERL A., VALENTE A., MELKOTE S., BRECHER C., OZTURK E., TUNC L.T., 2019, *Robots in Machining*, *CIRP Annals-Manufacturing Technology*, 68/2, 799–822, DOI: 10.1016/j.cirp.2019.05.009.
- [6] KAUSCHINGER B., FRIEDRICH C., ZHOU R., IHLENFELDT S., 2020, *Fast Evaluation of the Volumetric Motion Accuracy of Multi-Axis Machine Tools Using a Double-Ballbar*, *Journal of Machine Engineering*, 20/3, 44–62, DOI: 10.36897/jme/119678.
- [7] CHEN G., LI T., CHU M., XUAN J.-Q., XU S.-H., 2014, *Review on Kinematics Calibration Technology of Serial Robots*, *Int. J. Precis. Eng. Manuf.*, 15/8, 1759–1774, DOI: 10.1007/s12541-014-0528-1.
- [8] MESSAY T., ORDONEZ R., MARCIL E., 2016, *Computationally Efficient and Robust Kinematic Calibration Methodologies and Their Application to Industrial Robots*, *Robotics and Computer-Integrated Manufacturing*, 37, 33–48, DOI: 10.1016/j.rcim.2015.06.003.
- [9] HEXAGON ETALON, *ETALON LASERTRACER-NG – Etalon part of Hexagon*, <https://www.etalonproducts.com/en/products/lasertracer/> (accessed: Jan. 22 2022).
- [10] TOMITA M., IBARAKI S., 2020, *Measurement of 2D Positioning Error Map of a SCARA-Type Robot Over the Entire Workspace by Using a Laser Interferometer and a PSD Sensor*, *International Symposium on Flexible Automation*, Virtual, Online.
- [11] FILION A., JOUBAIR A., TAHAN A.S., BONEV I.A., 2018, *Robot Calibration Using a Portable Photogrammetry System*, *Robotics and Computer-Integrated Manufacturing*, 49, 77–87, DOI: 10.1016/j.rcim.2017.05.004.
- [12] NUBIOLA A., BONEV I.A., 2014, *Absolute Robot Calibration with a Single Telescoping Ballbar*, *Precision Engineering*, 38/3, 472–480, DOI: 10.1016/j.precisioneng.2014.01.001.
- [13] API, *Kabelloser Ballbar*, <https://apimetrolgy.com/de/ballbar/> (accessed: Feb. 21 2022).
- [14] ZIEGERT J.C., MIZE C.D., 1994, *The Laser Ball Bar: A New Instrument for Machine Tool Metrology*, *Precision Engineering*, 16/4, 259–267, DOI: 10.1016/0141-6359(94)90002-7.
- [15] BROSED F. J., AGUILAR J. J., ACERO R., SANTOLARIA J., AGUADO S., PUEO M., 2022, *Calibration and Uncertainty Budget Analysis of a High Precision Telescopic Instrument For Simultaneous Laser Multilateration*, *Measurement*, 190, 110735, DOI: 10.1016/j.measurement.2022.110735.
- [16] ZHOU R., KAUSCHINGER B., IHLENFELDT S., 2021, *Data Synchronization by Continuous Spatial Measurement with Double Ballbar*, *Measurement*, 174, 108909, DOI: 10.1016/j.measurement.2020.108909.
- [17] ZHOU R., KAUSCHINGER B., IHLENFELDT S., 2020, *Path Generation and Optimization for DBB Measurement with Continuous Data Capture*, *Measurement*, 155, 107550, DOI: 10.1016/j.measurement.2020.107550.
- [18] FRIEDRICH C., KAUSCHINGER B., IHLENFELDT S., 2020, *Stiffness Evaluation of a Hexapod Machine Tool with Integrated Force Sensors*, *Journal of Machine Engineering*, 20/1, 58–69.
- [19] GARNIER S., SUBRIN K., 2022, *A Metrological Device for Robot Identification*, *Robotics and Computer-Integrated Manufacturing*, 73, 102249, DOI: 10.1016/j.rcim.2021.102249.
- [20] ARCHENTI A., 2011, *A Computational Framework for Control of Machining System Capability: from Formulation to Implementation*, KTH Royal Institute of Technology.
- [21] ARCHENTI A., NICOLESCU M., CASTERMAN G., HJELM S., 2012, *A New Method for Circular Testing of Machine Tools Under Loaded Condition*, *Procedia CIRP*, 1, 575–580, DOI: 10.1016/j.procir.2012.05.002.
- [22] THEISSEN N.A., 2021, *Precision Measurement Instruments for Machinery's Mechanical Compliance: Design and Operation*, *Measurement Instruments for Physics-Based Calibration of Advanced Manufacturing Machinery*, KTH, Production Engineering.
- [23] LASPAS T., 2018, *Closed Force Loop Evaluation of Machining Systems*, TRITA-ITM-AVL, ISBN 978-91-7729-809-0.
- [24] DENAVIT J., HARTENBERG R.S., 1955, *A Kinematic Notation for Lower-Pair Mechanisms Based on Matrices*, *J. Appl. Mech.*, 22/2, 215–221, DOI: 10.1115/1.4011045
- [25] SCHRÖER K., 1993, *Theory of Kinematic Modelling and Numerical Procedures for Robot Calibration*, *Robot Calibration*, 157196, 44.

-
- [26] SICILIANO B., KHATIB O., 2016, *Springer Handbook of Robotics*, DOI: 10.1007/978-3-319-32552-1.
- [27] DANAY D., PAPEGAY Y., MADELINE B., 2005, *Choosing Measurement Poses for Robot Calibration with the Local Convergence Method and Tabu Search*, *The International Journal of Robotics Research*, 24/6, 501–518, DOI: 10.1177/0278364905053185.
- [28] COOK W.J., APPLGATE D.L., BIXBY R.E., CHVATAL V., 2011, *The Traveling Salesman Problem*, Princeton University Press.
- [29] THEISSEN N.A., GONZALEZ M.K., BARRIOS A., ARCHENTI A., 2021, *Quasi-Static Compliance Calibration of Serial Articulated Industrial Manipulators*, *Int. J. Automation Technol.*, 15/5, 590–598, DOI: 10.20965/ijat.2021.p0590.
- [30] SCHELLEKENS P., ROSIELLE N., VERMEULEN H., VERMEULEN M., WETZELS S., PRIL W., 1998, *Design for Precision: Current Status and Trends*, *CIRP Annals-Manufacturing Technology*, 47/2, 557–586, DOI: 10.1016/S0007-8506(07)63243-0.
- [31] GONZALEZ M., HOSSEINI A., THEISSEN N.A., ARCHENTI A., 2020, *Quasi-Static Loaded Circular Testing of Serial Articulated Industrial Manipulators*, *ISR*, 52th International Symposium on Robotics, 1–6.
- [32] ARCHENTI A., NICOLESCU M., 2013, *Accuracy Analysis of Machine Tools Using Elastically Linked Systems*, *CIRP Annals-Manufacturing Technology*, 62/1, 503–506, DOI: 10.1016/j.cirp.2013.03.100.
- [33] SLOCUM A.H., 1992, *Precision Machine Design*, ISBN-10: 0872634922.